Journal of Thermal Analysis, Vol. 58 (1999) 153-165

PYRAZINE COMPLEXES OF OCTACYANOMETALLATES OF Mo(IV) AND W(IV) WITH 8-HYDROXYQUINOLINE
Synthesis, characterisation and thermal studies

S. I. Ali and K. Majid*

Department of Chemistry, Jamia Millia Islamia, New Delhi 110 025, India

(Received February 10, 1998; in revised form November 10, 1998)

Abstract

The complexes formed by photosubstitution of pyrazine (Pz) in octacyanomolybdate(IV) and -tungstate(IV) with 8-hydroxyquinoline have been assigned the formulae $[Mo(CN)_2(OH)_2(Pz)_2(OX)]$ and $[W(CN)_2(OH)_2(Pz)_2(OX)\cdot 1.5H_2O]$. Coordination of Pz as a unidentate ligand by donating a lone pair of electron from nitrogen is shown by an absorption peak between 8–11 μ. Mechanism for the thermal decomposition of the complexes has been given. The formation of tungsten metal as residue in case of II has been confirmed by XRD analysis. The kinetic and thermodynamic parameters like activation energy (E_a), pre-exponential factor (A) and entropy of activation ($\Delta S^{\#}$) were calculated employing different integral methods of Doyle, Coats and Redfern and Arrhenius. ΔH for each stage of decomposition was obtained from DSC.

Keywords: metal-8-hydroxyquinoline complexes, photosubstitution of pyrazine, octacyanometallates, thermal dissociation

Introduction

Pyrazine (Pz) is known to form a variety of complexes with different transition metals in which it acts as bridging ligand [1], chelating ligand [2] and also bidentate ligand [3]. The kinetics and thermodynamic properties of different transition metals containing pyrazine and substituted Pz have been studied because of possible formation of inorganic polymers, their availability and their thermal stabilities [4–6]. The thermal study of Pz compounds with first row transition elements has been reported in which the spectral and other characterization methods have been employed to interpret the type of coordination which takes place with the metal ion [7–8].

The other aspect of the current study is the knowledge of quinones, the hydroxy quinones and their coordination compounds which are known to possess numerous chemically and biologically significant properties [9–13]. Thermal investigation on the chelate complexes of hydroxy-quinolines with bivalent metals have been reported [14]. The thermal behaviour of photoproducts of molybdenum(IV and V) and tungsten(IV and V) with oxine has been reported [15–16]. The thermal and kinetic

* Author to whom all correspondence should be addressed.

1418–2874/99/ $ 5.00

Akadémiai Kiadó, Budapest
Kluwer Academic Publishers, Dordrecht

study of photosubstituted octacyanometallates of molybdenum(IV) and tungsten(IV) with different ligands like ethylenediamine, triethylenetetramine and 1,2,3-benzotriazole forming adducts with 8-hydroxyquinoline have been reported [17–18].

Keeping in view the interesting and peculiar binding of pyrazine and 8-hydroxyquinoline, the title study was undertaken to investigate the thermal behaviour and mode of coordination of photosubstituted Pz on complexation with a chelating agent, 8-hydroxyquinoline. The complexes have been characterized by IR and thermal analysis. Mechanism for thermal decomposition of complexes has been given. Thermodynamic parameters like activation energy (E_a), pre-exponential factor (A) and entropy of activation ($\Delta S^{\#}$) have been calculated.

Experimental

Materials and methods

Potassium octacyanomolybdate(IV) and -tungstate(IV) were prepared by the method of Leipoldt *et al.* [19]. Pz was of AR grade provided by Sigma Chemical Company. The solution of 8-hydroxyquinoline was prepared by dissolving 2.0 g of AR oxine in 100 ml of 2.0 M acetic acid, ammonia was added dropwise to neutralise the acid. The turbidity produced in the solution was removed by adding one drop of acetic acid [20].

Synthesis of complexes

The complexes were synthesized by irradiating $K_4[M(CN)_8]$ [where M=Mo(IV) or W(IV)] and Pz solutions of 0.1 M strength in 1:2 ratio under UV light, till the color of the solution changed to deep red. Irradiation was stopped at that stage and solution of 8-hydroxyquinoline was added till greenish precipitate in both the cases were obtained. The precipitates were washed with water and ethanol and dried over fused $CaCl_2$. The complexes were analysed for C, H, N and metal. The formula for molybdenum complex was found to be

$Mo(CN)_2(OH)_2(C_4H_4N_2)_2(C_9H_7ON)$ **I** for which the observed percentage of C, H, N and Mo is 46.8, 1.7, 19.5 and 19.6 vs. calculated 46.8, 1.4, 20.1 and 23.0. The formula for tungsten analog is $W(CN)_2(OH)_2(C_4H_4N_2)_2(C_9H_7ON)\cdot 1.5\ H_2O$ **II**. The observed percentage of C, H, N and W is 37.5, 3.0, 15.6 and 29.8 *vs*. calculated values 37.2, 3.3, 16.2 and 30.5.

Physical measurements

Determination of carbon, hydrogen and nitrogen was carried out by micro analytical methods. IR spectra of the complexes were recorded on Perkin Elmer 1710 Fourier transform spectrophotometer in the range of 4000–400 cm^{-1} using KBr discs technique. The TG was conducted on DuPont 2000 thermal analyser. DSC was also carried on DuPont 2000 TA system with a differential scanning calorimeter.

The scanning was done at a rate of 10°C min^{-1}. An aluminium pan was used as reference under dynamic nitrogen atmosphere. The instrument calibration was checked by the samples of indium (99.99%) purity. XRD was done at an ambient temperature on a Philips-Holland XRD unit Model No: Ph 1130/00 using CuK_α radiation (λ=1.5405 Ĺ) at a scanning speed of 1° min^{-1}.

Table 1 FTIR spectral frequencies with their assigments for $[Mo(CN)_2(OH)_2(C_4H_4N_2)_2(C_9H_7ON)]$ **I** and $[W(CN)_2(OH)_2(C_4H_4N_2)_2(C_9H_7ON)\cdot 1.5H_2O]$ **II**[a]

Frequency/cm^{-1} Complex **I**	Assignment	Frequency/cm^{-1} Complex **II**	Assignment
3400(s)	ν(OH)	3400(s)	ν(OH)
		3040(s)	ν(OH)
3040(s)	ν(OH)	2560(s)	ν(N–H)
2400(s)	ν(N–H)	2120(s)	ν(C≡N)
2100(s)	ν(C≡N)	2080(s)	ν(C≡N)
1600(s)	ν(=N–H)	1640(s)	δ(NH_2)
	(H–O–H) bending		
1460(s)	ν_{sym}(C=O)	1600(s)	ν(=N–H)
			(H–O–H) bending
1380(s)	ν(–N=N–)	1560(s)	ν(N=H) bending or
			ν(C–N)
1320(vs)	ν_{sym}(C–O)	1500(s)	ν(N=O) or ring vib.
1260(vs)	ν(N–O) due to Pz	1460(s)	ν_{sym}(C=O)
1240(s)	ν(N=O)	1400(s)	ν(–N=N–)
1180(s)	asym. ring vibration	1300(s)	ν_{sym}(C–O)
1100(vs)	ν(C–O) of oxine or Pz	1260(s)	ν(–C–N) or
			ν(–N=O) due to Pz
900(vs)	vibration due to Pz	1200(m)	ν(–N=O)
800(m)	ν(N–O)	1080(m)	ν(M–O–H)
840(vs)	Mo–O stretching	1040(m)	ν(N–O) of oxine
760(vs)	C–H bond	1000(m)	ν(C–O)
640(m)	ν(C–O–Mo–O)	800(m)	ν(W=O)
540(s)	δ_{sym}(C–C–O)	760(s)	C–H bond
500(s)	metal–ligand	660(m)	ν(C–O–W–O)
		540(m)	δ_{sym}(O–C–O)
		480(m)	metal–ligand
			ν(M–N)

Results and discussion

The photoinitiated complexation and kinetics of octacyanometallates of molybdenum(IV) and tungsten(IV) with Pz which behaves as an unidentate ligand has been reported [21]. The substituted complexes of Pz with 8-hydroxyquinoline have been synthesized and characterized by IR and thermal analysis. IR absorption bands confirm the presence of coordinating moieties by various characteristic peaks and contributes towards understanding the behaviour of Pz with the metal in the solid complexes. The position and the assignment of IR absorption peaks of both the complexes is shown in Table 1. The strong absorption peak at 3400 cm^{-1} is shown by both the complexes due to O–H stretching vibration showing the presence of hydroxyl group. The presence of the coordinated water in **II** is shown by rocking, twisting and wagging mode of water coordinated to metal in the lower frequency region at 760 and 720 cm^{-1}. Generally aromatic C–H stretching vibrations occur at 3100 to 3000 cm^{-1}, this aromatic C–H stretching bands at 3040 cm^{-1} (vs) are fund for both the complexes. Complexes in which Pz is bonded through only one of its nitrogen atoms, an extra absorption bands is found in the region between 1250–909 cm^{-1} [22]. The appearance of absorption bands due to aromatic ring Pz are at 1180 (vs) cm^{-1}, 1100 (vs) cm^{-1} in the complex **I** and at 1000 (s), 1040 (m), 1080 (m) cm^{-1} in complex **II**, and the appearance of very strong absorption bands at 900, 1240 cm^{-1} in **I** and at 1280 cm^{-1} in **II** attributes towards monodentate behaviour of Pz. The appearance of the strong absorption peaks at 2100 cm^{-1} (vs) and 2120 cm^{-1} (vs) in **I** and **II** respectively shows the presence of cyanide as ν(–C≡N).

The cyanide peak in octacyanomolybdate(IV) is at 2070 cm^{-1} [23], thus in complexes **I** and **II** it is shifted to the higher frequency by 30 and 50 cm^{-1} respectively. In complex **II** another peak at 2080 (s) cm^{-1}, implies the presence of cyano group with the mode *M*–C≡N. The coordination of the 8-hydroxyquinoline with octacyanometallates of molybdenum(IV) and tungsten(IV) shows the frequency band at 1569 cm^{-1} (s) and 1554 cm^{-1} (vs) respectively due to the ν(C=N) stretching [24]. This type of frequency is present in complex **II** at 1560 (vs) cm^{-1}, 1500 (s) cm^{-1} which is attributed due to ν(C=N). Free oxine exhibits ν(N=O) at 1050 cm^{-1}, besides absorption peaks due to ν(C–O) and ν(N–O). The absorption peaks in complex **I** due to oxine are at 1460 (s), 1380, 1320, 110 (vs) cm^{-1} assigned as ν_{asym}(C=O), ν(N=N), ν_{asym}(C–O), ν(–C–O) respectively, in complex **II**, the absorption band due to ν(–C=O) of oxine is at the same position, the bands due to ν(–N=N) undergo a shift of 20 cm^{-1} towards higher frequency and the band due to ν_{asym}(C–O) shows a shift of 20 cm^{-1} towards lower frequency region from that of **I**. The region between 450–110 cm^{-1} is very significant in which the absorption bands due to *M*–O modes appear. In complex **I** the absorption bands at 500 (s) cm^{-1} shows metal–ligand bond, 540 (s) cm^{-1} due to δ_{sym}(C–C–O), 760 (s) cm^{-1} due to ν(C–H). The band at 840 (vs) cm^{-1} in complex **I** and 800 (vs) cm^{-1} in complex **II** is assigned to *M*=O stretching. The absorption bands due to C–H appear at the same position on 760 (s) in both the complexes. In complex **I**, other lower frequency bands appear at 640 (m), 540 (s) and 500 (s) assigned as ν(C–O–Mo–O), δ_{sym}(C–C–O) and metal–ligand while the same appear in **II** at 660 (m), 540 (m) and 480 (m) respectively.

Thermal analysis

$[Mo(CN)_2(OH)_2(C_4H_4N_2)_2(C_9H_7ON)]$ **I**

The thermal analysis curves (TG/DTG) are shown in Fig. 1. The temperature ranges and percentage mass losses of the decomposition are given in Table 2. The

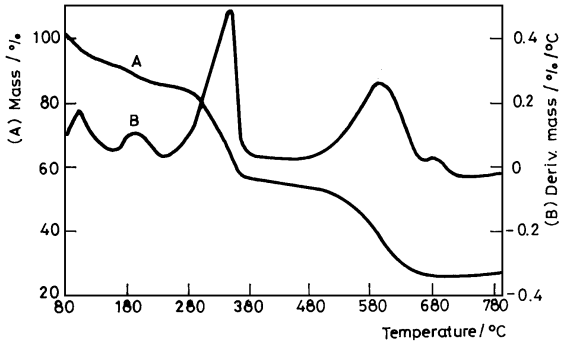

Fig. 1 The TG and DTG curves of **I**

Table 2 Thermoanalytical data for the decomposition of the complexes: $[Mo(CN)_2(OH)_2(C_4H_4N_2)_2(C_9H_7ON)]$ **I** and $[W(CN)_2(OH)_2(C_4H_4N_2)_2(C_9H_7ON)\cdot 1.5H_2O]$ **II**

$T_{DTG\ range}$/ °C	$T_{DTG\ max}$/ °C	Mass loss/% obs.	Mass loss/% calc.	Remarks removal of
Complex **I**				
90–180	105.1	9.54	10.6	2 moles of CN
180–280	186.0	7.0	6.9	2 moles of OH
290–361	349.8	29.5	29.7	1 mole of oxine
380–750	597.7	30.7	32.8	2 moles of Pz
				residue is Mo metal calc.%(19.68) obs.%(23.06)
Complex **II**				
105–134	125.9	4.8	4.4	1.5 moles of H_2O
175–245	210.2	38.2	37.4	1 mole of oxine+ 1 mole of Pz
258–279	270.6	5.2	5.6	2 moles of OH
300–380	347.0	13.2	13.2	1 mole of Pz
460–510	491.5	8.4	8.6	2 moles of CN
				residue W metal calc.%(30.5) obs.%(29.8)

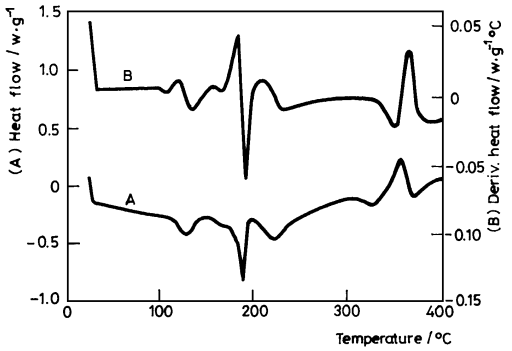

Fig. 2 The DSC curves of **I**

thermal decomposition takes place in four steps. The complex is stable upto 90°C showing no loss in mass, confirming the complex to be anhydrous as generally uncoordinated water is removed below 100°C. The two moles of cyanide are lost at 90–180°C, with the DTG maximum at 105.1°C. The observed mass loss is 9.54 compared with calculated 10.67%. This step is followed by a second deep step initiating from 180–280°C with a DTG maximum of 186.0°C. The observed mass loss is 7.05 *vs.* calculated 6.97% which is due to the release of two hydroxide moieties. The two steps are not distinguished from TG due to immediate initiation of second step but the DTG curve demarcates the two transitions quite clearly. The third step initiated from 290 up to 361°C undergoing a significant mass loss of 29.56 *vs.* calculated 29.78% due to the removal of a molecule of 8-hydroxyquinoline (oxine). The DTG maximum is at 349.8°C. The complex then does not undergo any change upto 380°C after which it starts its fourth decomposition step which continues up to 750°C with DTG maximum of 597.73°C, involving the mass loss of 30.79 compared to calculated 32.87% due to loss of two moles of Pz. The observed percentage of residue is 23.06 which is due to Mo metal, the calculated percentage of which is 19.68. The DSC of the complex carried out in nitrogen atmosphere from room temperature to 500°C is shown in Fig. 2. The curve shows four transitions, three exothermic and one endothermic corresponding to four mass loss ranges observed in TG curve. The first exothermic transition starts from 116.37 and stops at 151.44°C with maximum of 127.93°C giving ΔH value of 14.96 J g^{-1}. The second transition starts from 160.3 and continues upto 199.52 with maximum of 188.43°C giving ΔH of 28.83 J g^{-1}. The second transition is followed by the similar type of transition initiating from 205.9 upto 268.0 with maximum of 223.1°C giving ΔH value of 27.45 J g^{-1}. The last transition starts from 323.76 up to 375.0 with maximum of 357.5°C giving ΔH value of 38.41 J g^{-1}. The maximum value of ΔH is observed in the last transition confirming the TG decomposition processes of evolving bulky group of two moles of Pz, thus showing the higher thermal stability and greater coordination with the Mo atom. The sequential thermal decomposition steps of TG and DTG are shown in Scheme **I**. The calculated and observed values are represented with or without parentheses respectively.

Scheme **I**:

$$[Mo(CN)_2(OH)_2(Pz)_2(OX)] \xrightarrow[9.45]{(10.67)} [Mo(OH)_2(Pz)_2(OX)] +$$

$$+ 2CN(\Delta H = 14.96\ J\ g^{-1}) \xrightarrow[7.05]{(6.97)} [Mo(Pz)_2(OX)] + 2OH(\Delta H = 28.83\ J\ g^{-1})$$

$$\xrightarrow[29.56]{(29.78)} [Mo(Pz)_2] + (OX)(\Delta H = 27.45\ J\ g^{-1})$$

$$\xrightarrow[30.79]{(32.87)} Mo + 2Pz(23.06);\ 19.68\%\Delta H = 38.41\ J\ g^{-1}$$

$[W(CN)_2(OH)_2(C_4H_4N_2)_2(C_9H_7ON)\cdot 1.5H_2O]$ **II**

The TG/DTG of the tungsten analog is shown in Fig. 3. The stoichiometry of the complex is similar to that of the Mo(IV) except presence of coordinated water, which is shown by IR absorption peaks due to rocking, twisting and waging modes of water besides fundamental vibrations. The loss of 1.5 moles of coordinated water starts from 105 and continues up to 134.15 with DTG maximum of 125.9°C. The temperature range and DTG maximum justifies the presence of water as a coordinat-

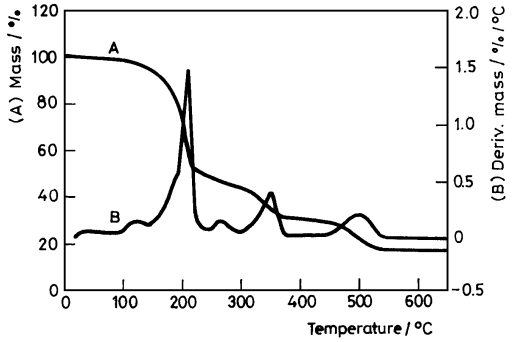

Fig. 3 The TG and DTG curves of **II**

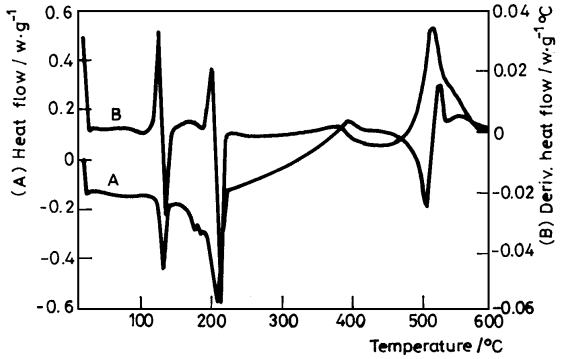

Fig. 4 The DSC curves of **II**

ing moiety. The observed mass loss is 4.89 as compared to calculated 4.48%. The rest of the decomposition takes place in four steps supporting the rest of the complex similar to that of the Mo(IV), but the order of the release of the moieties is just the reverse of the order as in molybdenum case. The second mass loss step starts from 175.0 and continues up to 245 with DTG maximum of 210.2°C involving the loss of 1 mole of Pz and one mole of oxine. The observed mass loss is 38.29% *vs.* calculated 37.40. The continuity of first and second transition does not make the demarcation of the two separate steps in TG curves but the DTG curve shows the transitions significantly. The next stage of decomposition starts from 258 and ends at 279 with DTG maximum at 270.6°C and is due to the release of two moles of hydroxyl groups. The observed mass loss is 5.29 as compared to calculated 5.60%. This transition is followed by the loss of one mole of pyrazine which onsets from 300 and ends at 380 with DTG maximum of 347°C involving the observed mass loss of 13.23% as compared to calculated 13.29. The last mass loss step starts from 460 and continues upto 510 with DTG maximum of 491.5°C, this involves loss of two moles of cyanide with observed mass loss of 8.45 *vs.* calculated 8.63%. The complex was subjected to treatment upto 800 but no change was found after 510°C. The residue was found 29.85 *vs*. calculated 30.52% due to metal tungsten. The DSC of the complex is shown in Fig. 4. The curve shows two exothermic and one endothermic transitions. The first transition starts from 109.22 up to 162.8 with maximum at 136.18°C. The heat of reaction involved is 12.85 J g^{-1}. The second transition starts from 187.97 upto 230.32 with maximum at 198.02°C involving ΔH value of 38.08 J g^{-1}. The third endothermic transition starts from 466.41 up to 584.6 with maximum at 516.95°C involve overlapping of other transitions also because of the significant value of ΔH 109 J g^{-1}. The maximum value of enthalpy observed in this stage justifies the higher stability and greater coordination of corresponding moieties with the central W atom. The thermal decomposition steps involved are shown in Scheme **II**. The calculated and observed mass loss is represented with and without parentheses respectively.

Scheme **II**:

$$[W(CN)_2(OH)_2(Pz)_2(OX)\cdot 1.5H_2O] \xrightarrow[4.89]{(4.48)} [W(OH)_2(Pz)_2(OX)] +$$

$$+ 1.5H_2O(\Delta H{=}12.85\ J\ g^{-1}) \xrightarrow[38.29]{(37.4)} [W(CN)_2(OH)_2(Pz)] + Pz +$$

$$+ OX(\Delta H{=}38.08\ J\ g^{-1}) \xrightarrow[5.29]{(5.60)} [W(CN)_2(Pz)] + 2OH \xrightarrow[13.23]{(13.29)}$$

$$[W(CN)_2] + Pz(\Delta H{=}109.1\ J\ g^{-1}) \xrightarrow[8.45]{(8.63)} W + 2CN(29.85);30.52$$

XRD analysis

The interplanar 'd' spacings of the residue of **II** were determined and found to be in accordance with the reported data for the W metal.

Observed		ASTM File W-4-806	
d/Ĺ	**I**/%	*d*/Ĺ	**I**/%
2.238	100	2.238	100
1.582	60	1.582	15
1.292	40	1.292	23

Mo complex **I** loses CN in the first step whereas in tungsten analog **II**, CN is lost in the final step showing that in **II** cyanide is strongly coordinated, hence removed at a higher temperature. The stronger coordination can be as a result of effective orbital mixing of metal and ligand which is influenced by two factors (1) the radial extension of the metal d orbitals and (2) energy difference, ΔE, between the metal orbitals and ligand (π^*) orbitals. Greater interaction is expected for the orbitals which are close in energy. The ability for metal–ligand orbital interaction is enhanced if the metal d orbitals extend far into space, enabling effective overlap with π^* (CN^-) orbitals of the ligand [25]. Since 5d orbitals are more close in energy than 4d orbitals, hence will extend more overlapping with π^* orbitals of ligand. Moreover the value

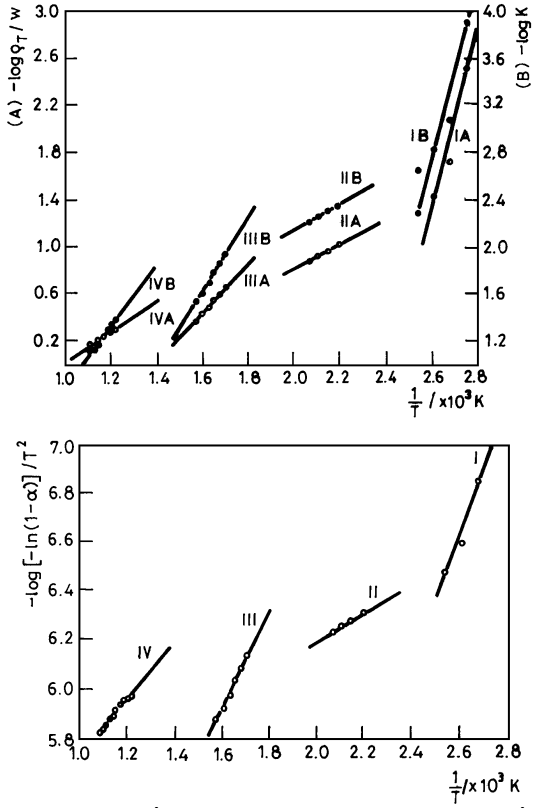

Fig. 5 Plot of $-\log\rho_T/w$ *vs.* $1/T\cdot10^3$ K of **I** (A) ; Plot of $-\log k$ *vs.* $1/T\cdot10^3$ K of **I** (B); Plot of $-\log[-\ln(1-\alpha)]/T^2$ *vs.* $1/T\cdot10^3$ K of **I** (C)

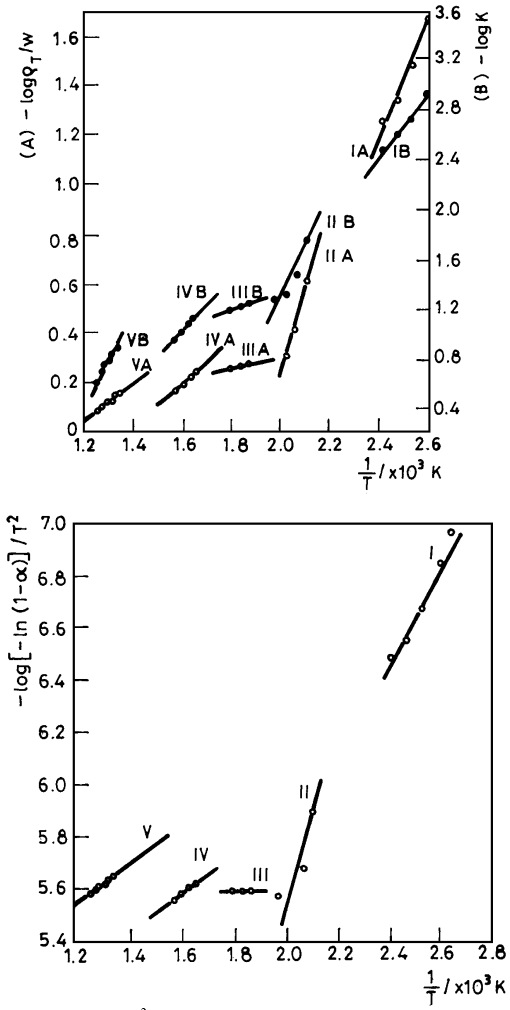

Fig. 6 Plot of $-\log\rho_T/w$ *vs.* $1/T{\cdot}10^3$ K of **II** (A); Plot of $-\log k$ *vs.* $1/T{\cdot}10^3$ K of **II** (B); Plot of $-\log[-\ln(1-\alpha)]/T^2$ *vs.* $1/T{\cdot}10^3$ K of **II** (C)

of the 10Dq increases when going from first to second transition series [26]. These considerations show that 5d orbitals have greater ability to form strong bond between metal and cyanide than 4d orbitals.

Kinetic parameters

Three different methods were employed for evaluation of kinetic data from these results. Thermodynamic parameters like activation energy (E_a), pre-exponential factor (A) and entropy of activation ($\Delta S^{\#}$) for different decomposition steps for complexes **I** and **II** are tabulated in Tables 3 and 4 respectively. Using Doyle's [27, 28] method modified by Reich and Stivale, reduction equation for degradation equation comes to be:

Table 3 Activation energy, frequency factor and entropy of activation for $[Mo(CN)_2(OH)_2(C_4H_4N_2)_2(C_9H_7ON)]$ **I**

Stage	Parameters	$T_{DTG\,max}$/K	Doyle	Coats and Redfern	Arrhenius
I	E_a/(kJ mol^{-1})		107.5	101.7	108.8
	A(s^{-1})	378.4	13.0	7.1	11.8
	$\Delta S^{\#}$(J k^{-1} mol^{-1})		–225.6	–230.6	–226.4
II	E_a/kJ mol^{-1}		18.8	11.7	20.9
	A(s^{-1})	459.0	1.2	4.9	0.04
	$\Delta S^{\#}$(J k^{-1} mol^{-1})		–247.2	–235.2	–275.2
III	E_a/kJ mol^{-1}		40.6	37.5	57.7
	A(s^{-1})	622.8	2.9	2.8	3.2
	$\Delta S^{\#}$(J k^{-1} mol^{-1})		–242.0	–242.5	–241.4
IV	E_a/kJ mol^{-1}		22.6	23.4	57.5
	A(s^{-1})	870.7	1.1	4.4	2.2
	$\Delta S^{\#}$(J k^{-1} mol^{-1})		–252.8	–241.4	–247.1

Table 4 Activation energy, frequency factor and entropy of activation for $[W(CN)_2(OH)_2(C_4H_4N_2)_2(C_9H_7ON)\cdot 1.5H_2O]$ **II**

Stage	Parameters	$T_{DTG\,max}$/K	Doyle	Coats and Redfern	Arrhenius
I	E_a/(kJ mol^{-1})		47.3	41.4	48.5
	A(s^{-1})	389.9	4.7	1.1	3.6
	$\Delta S^{\#}$(J k^{-1} mol^{-1})		–234.4	–245.9	–236.6
II	E_a/kJ mol^{-1}		44.8	47.7	69.0
	A(s^{-1})	483.2	4.3	0.5	5.8
	$\Delta S^{\#}$(J k^{-1} mol^{-1})		–236.7	–253.6	–234.2
III	E_a/kJ mol^{-1}		5.4	0.0	13.4
	A(s^{-1})	543.6	0.3	6.0	0.1
	$\Delta S^{\#}$(J k^{-1} mol^{-1})		–261.5	–235.7	–271.2
IV	E_a/kJ mol^{-1}		33.5	14.6	41.0
	A(s^{-1})	620.0	2.5	4.3	2.4
	$\Delta S^{\#}$(J k^{-1} mol^{-1})		–243.2	–238.9	–243.7
V	E_a/kJ mol^{-1}		14.2	14.6	52.3
	A(s^{-1})	764.5	0.8	40.6	2.7
	$\Delta S^{\#}$(J k^{-1} mol^{-1})		–254.2	–240.1	–244.3

$$\log\frac{\rho_T}{W}=\frac{E_a}{4.6T}+\log\frac{A}{(RH)} \text{ where } \rho_T=t/(RH)=-dw/dt \text{ and } (RH)=\text{heating rate}$$

On plotting $\log\rho_T/w$ *vs.* $1/T$, the value of E_a is obtained from the slope of the plot using the relation $E_a=-4.6x$ slope. The activation energies of **I** for four decomposition steps are 25.7, 4.5, 9.7, 5.4 kcal mol^{-1} and for five steps of **II** are 11.3, 10.7, 1.30, 8.0 and 3.4 kcal mol^{-1}. The pre-exponential factor (A) is obtained from the intercept of the plot and entropy of activation ($\Delta S^{\#}$) from a general equation:

$$A=\frac{kT_s}{h}\exp\frac{\Delta S^{\#}}{R} \qquad \text{(A)}$$

where k is the Boltzmann constant, h is the Plancks constant and T_s is the peak temperature. Using Coats and Redferns [29] method, the plot of $\log[-\ln(1-\alpha)]T^2$ *vs.* $1/T$ results in a straight line for a first order reaction with the slope $E_a/2.303R$. The value of A is obtained from the intercept of the plot and entropy of activation ($\Delta S^{\#}$) from the general equation (A). The activation energy values for **I** are 24.3, 2.8, 8.9 and 5.6 and for **II** are 9.9, 11.47, 0, 3.59, 3.53 kcal mol^{-1}. The activation energy was also determined from Arrhenius equation [30] by calculating the kinetic data from TG curve using the equation:

$$-dx/dt=kx^n$$

where x amount of the sample undergoing the reaction, n is the order of the reaction and k specific rate constant. On measuring k at several temperatures, graph of $\log k$ *vs.* $1/T$ gives a straight line whose slope is $-E_a/2.3R$ and intercept is 2.3 $\log A$. The activation energy values (E_a) for different four steps of **I** are 26.0, 5.0, 13.8 and 13.8 kcal mol^{-1} and for five steps of stage **II** are 11.6, 16.5, 3.23, 9.88, 12.58 kcal mol^{-1}.

From a comparative view, in complex **I** (Table 2), it is evident that greater the activation energy, greater is the entropy of activation. Negative values of entropy of activation indicate that the activated complexes have a more ordered structure and that the reactions are slower than the normal [31]. In complex **II** (Table 3), values from Coats and Redfern and Arrhenius method are more in agreement than Doyle's method, showing direct proportionality of activation energy and entropy of activation energy values. Lozano [32] found that the greater enthalpy and lower activation energy values are responsible for greater binding between pyridine and molybdenum atom in the complexes. Hence lower value of activation energy and entropy of activation shows strong coordination between the molecules. In complex **I**, the values of E_a and $\Delta S^{\#}$ is maximum for stage **I**, corresponding to the release of two moles of cyanide at the very beginning of thermal decomposition process, hence justifying the least binding with the central Mo atom. In complex **II** though the values from Coats and Redfern and Arrhenius are close in agreement, the values from Arrhenius are much more reliable, showing the maximum value of E_a and $\Delta S^{\#}$ for stage **I** corre-

sponding to the release of water at the very onset of thermal reactions justifying the least binding with W atom.

* * *

One of the authors Kowsar Majid is grateful to CSIR, New Delhi for the award of Senior Research Fellowship.

References

1 A. V. Kaneke, G. M. Tom and H. Taube, Inorg. Chem., 17 (1978) 7.
2 D. A. Edwards, G. Uden, W. S. Mialki and R. A. Walton, Inorg. Chim. Acta, 40 (1980) 25.
3 K. H. Pannell and R. Iglesias, Inorg. Chim. Acta, 33 (1979) 161.
4 T. G. Dunne and J. K. Hurst, Inorg. Chem., 19 (1980) 1152.
5 H. E. Toma and J. M. Malin, Inorg. Chem., 12 (1973) 9 and 2030.
6 J. R. Allan, A. D. Paton, K. Turvey, H. J. Bowely and D. L. Gerrard, Thermochim. Acta, 122 (1987) 403.
7 J. R. Allan, A. D. Paton, K. Turvey, H. J. Bowely and D. L. Gerrard, Thermochim. Acta, 124 (1988) 345.
8 J. R. Allan, H. J. Bowely, D. J. Gerrard, A. D. Paton and K. Turvey, Thermochim. Acta, 132 (1987) 41.
9 A. Dufrense, C. G. Delima, J. Kundsen and J. E. Moreira, J. Inorg. Nucl. Chem., 35 (1973) 789.
10 S. B. Padhye, C. R. Joshi and B. A. Kulkarni, J. Inorg. Nucl. Chem., 39 (1977) 1289.
11 P. H. Mezzell, Inorg. Chem. Acta, 32 (1979) 99.
12 S. Bratan and I. Strohbusch, J. Mol. Struct., 61 (1980) 409.
13 M. S. Masoud, E. M. Sloiman and M. E. El. Shabasy, Thermochim. Acta, 125 (1988) 9.
14 M. Lalia-kantouri, M. Bakola-Chiristianopoulou, Thermochim. Acta, 104 (1986) 39.
15 S. I. Ali and N. K. S. Pundhir, Thermochim. Acta, 224 (1993) 247.
16 S. I. Ali and N. K. S. Pundhir, Thermochim. Acta, 38 (1992) 1391.
17 S. I. Ali, A. M. A. Ansari and N. K. S. Pundhir, Indian J. Chem. (sec A) 34 (1995) 423.
18 S. I. Ali and A. M. A. Ansari, J. Thermal Anal,. 46 (1996) 1763.
19 L. G. Leipoldt, L. D. C. Bok and P. G. Colliers, Z. Anorg. Allgem. Chem., 409 (1974) 343, 407 (1974) 250.
20 A. I. Vogel, A Textbook of Qualitative Inorganic Analysis, Longman, London 1982.
21 S. I. Ali and Kowsar Majid, Transition Met. Chem., 22 (1997) 309.
22 A. B. P. Lever, J. Lewis and R. S. Nyholm, J. Chem. Soc., (A), (1962) 1235.
23 F. A. Kettle and R. V. Parsish, Spectrochim. Acta, 21 (1965) 1087.
24 S. I. Ali and N. K. S. Pundhir, Thermochim. Acta, 189 (1991) 68.
25 C. R. Johnson and R. E. Shephered, Inorg. Chem., 22 (1983) 2439.
26 J. A. Olabe, H. O. Zerga and L. A. Gentil, J. Chem. Soc. Dalton Trans., (1987) 1267.
27 C. D. Doyle, J. Appl. Polymer. Sci., 5 (1961) 285.
28 C. D. Doyle, Anal. Chem., 33 (1961) 77.
29 A. W. Coats and J. P. Redfern, Nature, 201 (1964) 68.
30 J. R. Hullet, Quart. Rev., 18 (1964) 227.
31 A. A. Frost and R. G. Pearson, Kinetics and Mechanism, Wiley, New York 1961, p. 101.
32 R. Lozano, A. Moragues and J. Romans, Thermochim. Acta, 108 (1986) 1.